Journal of Soil Science and Plant Nutrition
https://doi.org/10.1007/s42729-024-01846-2

ORIGINAL PAPER

Spatiotemporal Characteristics of Soil Erosion on the Chinese Loess Plateau and Strategies for Vegetation Management

Wanghai Tao[1] · Shiyao Liu[1] · Quanjiu Wang[1] · Lijun Su[1] · Yan Sun[1]

Received: 31 October 2023 / Accepted: 29 May 2024

Abstract
The Chinese Loess Plateau plays a crucial role in soil and water conservation and ecological restoration. China has implemented the Grain for Green project since the year 2000 to address the problem of soil erosion in the aforementioned region. This study aims to evaluate the effectiveness of the Grain for Green project by analyzing the temporal and spatial changes in soil erosion on the Loess Plateau from the year 2000 to 2021. The spatiotemporal characteristics of soil erosion on the Loess Plateau were evaluated from both water and wind erosion perspectives. The Revised Universal Soil Loss Equation (RUSLE) was used for water erosion assessment, while the Revised Wind Erosion Equation (RWEQ) was used for wind erosion assessment. The average annual water and wind erosion intensities were 14.56 and 3.95 $t{\cdot}ha^{-1}{\cdot}yr^{-1}$, respectively, during the study period. Vegetation coverage, erosive rainfall, and erosive wind intensity showed an increasing trend, while the conversion of land use types primarily involved transforming cropland, bare land, and shrubland into forest and grassland. The comprehensive dynamic changes in various factors resulted in a considerable decrease in water erosion, while wind erosion did not exhibit a remarkable trend over time. Overall, the Grain for Green project has achieved remarkable effectiveness. Increasing vegetation coverage in each subregion is recommended to control soil erosion further, with specific recommended increments as follows: Gully region (4.29%), Hilly–gully region (3.27%), Valley Plain region (2.18%), Earth–rock Mountain region (2.86%), Irrigation region (1.21%), and Sandy region (1.00%). Under optimized vegetation coverage conditions, the intensities of water and wind erosion decreased by 72.03% and 7.20%, respectively. However, 18.50% of the region still experienced water erosion intensity, and 6.72% experienced wind erosion intensity, which reached extremely slight or high levels. Therefore, these areas may require additional soil conservation measures to address soil erosion issues. Specific measures should be tailored to the actual conditions and be in accordance with the overall goals of Loess Plateau management and the development needs of the Yellow River Basin.

Keywords Chinese loess plateau · Grain for green project · Soil erosion · Ecological restoration

1 Introduction

The Chinese Loess Plateau is the largest loess accumulation area in the world, and it is characterized by continuous Quaternary loess deposits. In the gully and hilly–gully regions, the thickness of loess generally ranges from 100 m to 300 m. As a result, it is heavily affected by widespread soil erosion, which makes it one of the most severely affected regions in the world in terms of water and soil erosion. The Loess Plateau is a popular area in China and is known to have severe soil erosion. It plays a crucial role in contributing (97%) to the sediment load of the Yellow River. Loose soil, steep slopes, sparse vegetation, and specific climatic conditions, including solid spring winds and heavy summer rainfall, have resulted in extensive soil erosion on the Loess Plateau (Guo and Shao 2019; Sun et al. 2014). The consequences of this soil erosion are not limited to the ecological system and water quality of the Yellow River. They also pose considerable challenges to downstream areas regarding water resource management, river engineering, and flood control measures (Shi and Shao 2000). Implementing

Wanghai Tao and Shiyao Liu contributed equally to this work.

✉ Wanghai Tao
xautsoilwater@163.com

[1] State Key Laboratory of Eco-hydraulics in Northwest Arid Region, Xi'an University of Technology, Xi'an 710048, China

Published online: 14 June 2024

effective methods for anticipating and mitigating soil erosion is crucial to enhancing crop productivity and restore ecosystems.

The Revised Universal Soil Loss Equation (RUSLE), which was developed by Wischmeier and Smith (1978), is a widely used model for simulating water erosion. It is known for its simplicity and ability to work with limited data. Numerous studies have shown the accuracy and reliability of the RUSLE model results. Another commonly used model for soil erosion is the Revised Wind Erosion Equation (RWEQ), which was introduced by Fryrear et al. (2000). This model has a simple structure, uses easily obtainable parameters, and can assess the spatial and temporal variations of wind erosion without extensive fieldwork. It is a valuable tool for studying wind erosion processes and predicting wind erosion risks. These soil erosion models have various applications. For example, the RUSLE model can be used by researchers to evaluate the effect of different land use practices on soil erosion and develop corresponding land management measures (Fu et al. 2011; Li et al. 2020). It can also assess the effectiveness of land use policies and inform environmental protection policies. Meanwhile, the RWEQ model can be used to assess the spatial distribution and trends of wind erosion, which provides a scientific basis for wind erosion control. The application of these models helps guide agricultural production, land planning, and natural resource management (Fryrear et al. 2000). It reduces the adverse effects of soil erosion on the environment and socioeconomics, thereby promoting sustainable land use and ecological protection. Google Earth Engine (GEE) (Gorelick et al. 2017) is a powerful analysis tool for regional soil erosion. For example, Elnashar et al. (2021) developed the RUSLE–GEE framework to assess water erosion in the Blue Nile Basin, while Wang et al. (2020) used the GEE–RWEQ method to evaluate wind erosion in Central Asia. These studies effectively utilized GEE to assess soil erosion. Following the implementation of the Grain for Green project, numerous scholars have investigated the dynamic changes in soil erosion across the Loess Plateau. Sun et al. (2014) evaluated the spatial and temporal characteristics of water erosion rates in the Loess Plateau from the year 2000 to 2010, and they explained the influence of different topographic and land use conditions on water erosion. Guo and Shao (2019) clarified the process of water erosion changes in the Loess Plateau from the year 2000 to 2015 and evaluated the role of human activities in water erosion changes and the effectiveness of ecological restoration projects. Xia et al. (2021) quantified the spatial and temporal characteristics of water erosion in the Yanwachuan watershed of the Loess Plateau and assessed the characteristics of land use change and climate change impacts on water erosion.

These scholars have used soil erosion models to evaluate the characteristics of water erosion dynamics in the Loess Plateau region after the implementation of the Grain for Green project. The characteristics of the influence of natural factors and human activities on water erosion have also been elucidated in different ways. Overall, these studies show that the Grain for Green project has made remarkable progress in mitigating soil erosion on the Loess Plateau. Notably, their findings have tended to focus only on studies of water erosion and have neglected to characterize the variability of the response to wind erosion. In addition, the effect of human activities on the ecological environment of the Loess Plateau has reached an unprecedented level (Guo et al. 2019; Li et al. 2019; Mu et al. 2022). Increasing vegetation cover is considered a highly effective forestry and grassland measure for mitigating soil erosion. In recent years, the Grain for Green project has remarkably boosted vegetation cover on the Loess Plateau, leading to a marked reduction in soil erosion, as mentioned in numerous scholarly studies. However, discussion regarding the ideal vegetation cover required to achieve a degradation in soil erosion intensity on the Loess Plateau is limited. Furthermore, as vegetation cover increases, the effectiveness of erosion control diminishes gradually, and solely relying on increasing vegetation cover cannot reduce soil erosion to zero. Hence, discussing the minimum achievable rate of soil erosion under ideal vegetation cover on the Loess Plateau is crucial to providing theoretical guidance for allocating other soil and water conservation measures.

This study comprehensively analyzes the soil erosion situation after the implementation of the Grain for Green project in the Loess Plateau. In this manner, the effects of relevant soil and water conservation measures can be systematically evaluated. In addition, it quantifies the maximum level of soil erosion intensity that can be reduced when the vegetation cover is increased to the ideal state, aiming to provide some theoretical basis for soil erosion control on the Loess Plateau. The details are as follows: (1) The spatiotemporal variations of soil erosion on the Loess Plateau from the year 2000 to 2021 are analyzed, and the soil erosion risk during different periods within a year is assessed. (2) The characteristic influences of various factors on dynamic soil erosion changes are elucidated. (3) Vegetation coverage enhancement plans for effective prevention of soil erosion in each subregion are proposed. (4) Soil erosion under ideal vegetation cover is quantified to provide theoretical guidance for rational allocation of soil and water conservation measures.

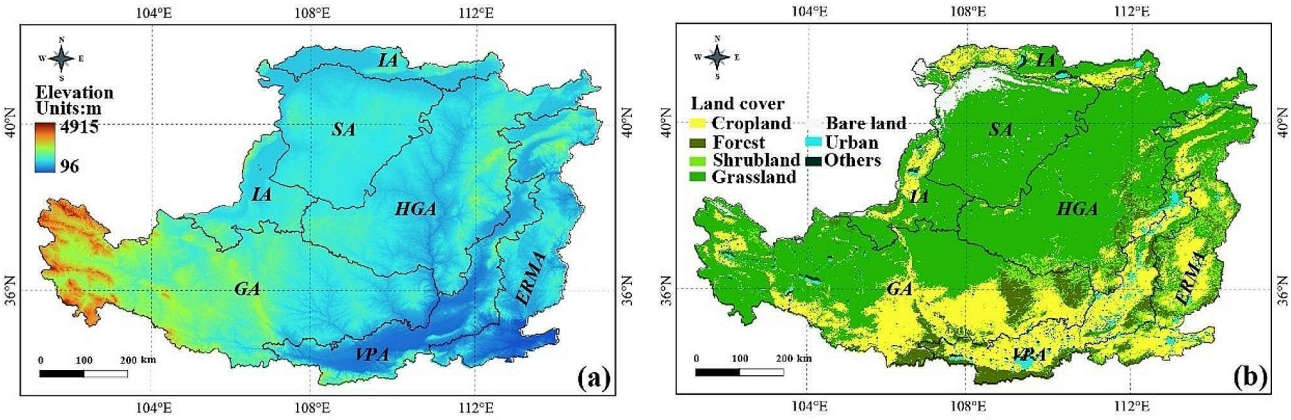

Fig. 1 Topography and land use patterns of the Chinese Loess Plateau. (**a**) and (**b**) depict the elevation and land cover of the Loess Plateau, respectively; GA is the Gully region, HGA is the Hilly–gully region, VPA is the Valley Plain region, ERMA is the Earth–rock Mountain region, SA is the Sandy region, and IA is the Irrigation region

Table 1 Dataset used for RUSLE and RWEQ modeling

Dataset	Period	Resolution	Source
Clay	-	250 m	SoilGrids
Sand	-	250 m	SoilGrids
Silt	-	250 m	SoilGrids
Organic carbon	-	250 m	SoilGrids
$CaCO_3$	-	0.083 degrees	HWSD
Land use	-	30 m	China Land Cover Dataset
NDVI	2000–2021	1000 m	MOD13A2.061
DEM	-	90 m	SRTM Digital Elevation Data Version 4
Precipitation-Daily	2000–2021	5566 m	CHIRPS Daily
Precipitation- Hourly	2000–2021	11,132 m	ERA5-Land Hourly
Wind speed	2000–2021	11,132 m	ERA5-Land Hourly
Potential evaporation	2000–2021	11,132 m	ERA5-Land Hourly
Temperature	2000–2021	11,132 m	ERA5-Land Hourly
Snow depth	2000–2021	0.25 degrees	GLDAS-2.1

2 Materials and Methods

2.1 Study Area

The Chinese Loess Plateau is situated in the northwestern part of China, and it covers a total area of 624,000 km^2 (Shi and Shao 2000). It is located at 33° N and 100° E. The region experienced brief but intense precipitation, which averaged between 200 and 750 mm over several years. Given its low water content and loose soil, the soil on the Loess Plateau has limited resistance to rain scouring and wind blowing, making it susceptible to water and wind erosion (Chen et al. 2007; Wen and Zhen 2020). The primary land use in this area includes cropland, forest, shrubland, grassland, bare land, and urban land. In this study, the Loess Plateau was divided into six subregions based on distinct topographic features and land use characteristics: Gully region, Hilly-gully region, Valley Plain region, Earth-rock Mountain region, Sandy region, and Irrigation region (Guo and Shao 2019). Figure 1 shows the topographical features, land use, and geographic zoning of the Loess Plateau.

2.2 Data Sources

The analysis and calculations for this study relied on various data sources, including meteorology, soil characteristics, elevation, vegetation index, and land use type (Table 1). Daily precipitation data were provided by the Climate Hazards Group InfraRed Precipitation with Station (5,566 m) (Funk et al. 2015). Snow-depth data with a temporal resolution of 3 h were obtained from the Global Land Data Assimilation System (0.25°). Wind speed, precipitation, potential evapotranspiration, and temperature data were obtained from ECMWF Climate Reanalysis (11,132 m) at an hourly temporal resolution (Muñoz Sabater 2019). Soil data, including soil organic carbon, clay, sand, and calcium carbonate, were sourced from SoilGrids and HWSD (Nachtergaele et al. 2009; Poggio et al. 2021). Digital elevation data were obtained from SRTM Digital Elevation Data Version 4 (90 m). The NDVI was obtained from MOD13A2 V6 product data (Didan 2021) produced by the USGS EROS Center. Land use data were obtained from the China Land Cover Dataset produced by Wuhan University (Yang and Huang 2021). All of the abovementioned raw data are in the uniform coordinate system of WGS_1984_ARC_System_Zone_02, and they were resampled to a uniform spatial resolution of 1000 m for subsequent computational analysis.

2.3 Research Methods

2.3.1 RUSLE Model

The RUSLE model (Wischmeier and Smith 1978) is an improved version of the USLE model (Wischmeier and Smith 1965). It established a statistical relationship between annual soil loss and six factors. The equation is as follows:

$$A = R \cdot K \cdot LS \cdot C \cdot P \tag{1}$$

where A is the average annual soil erosion ($t \cdot ha^{-1} \cdot yr^{-1}$); R is the rainfall erosivity factor ($MJ \cdot mm \cdot ha^{-1} \cdot h^{-1} \cdot yr^{-1}$); K is the soil erodibility factor ($t \cdot ha \cdot h \cdot ha^{-1} \cdot MJ^{-1} \cdot mm^{-1}$); LS is a topographic factor that combines slope length (L) and slope steepness (S) factors (unitless); C is the cover management factor (unitless); and P is the soil and water conservation factor (unitless).

(1) Rainfall erosivity factor (R)

The rainfall erosivity factor is a measure of the soil's susceptibility to erosion during a rainfall event. This factor is calculated by using an empirical equation based on daily rainfall (Zhang and Fu 2003). The equation for calculating the R factor for rainfall is shown as follows:

$$R = \alpha \sum_{j=1}^{k} (P_j)^{\beta} \tag{2}$$

$$\alpha = 21.586\beta^{-7.1891} \tag{3}$$

$$\beta = 0.8363 + \frac{18.144}{P_{d12}} + \frac{24.455}{P_{y12}} \tag{4}$$

where P_j is the erosive daily rainfall on the jth day of the semimonth (more than 12 mm of daily rainfall is required; otherwise, it is calculated as 0);α and β are parameters; P_{d12} is the average daily rainfall (daily rainfall greater than 12 mm); P_{y12} is the average annual rainfall (daily rainfall greater than 12 mm). Annual rainfall erosion force was obtained by summing the semimonthly rainfall erosivity.

(2) Soil erodibility factor (K)

Erosion resistance varies among different soil types, and the erodibility factor indicates the soil's susceptibility to erosion. One commonly used approach to determine soil erodibility is the EPIC model (Williams 1990):

$$K = 0.317 \times \left\{0.2 + 0.3\exp\left[-0.0256SAN\left(1 - \frac{SIL}{100}\right)\right]\right\}\left(\frac{SIL}{SIL+CLA}\right)^{0.3} \times \left[1 - \frac{0.25OC}{OC+\exp(3.72-2.95OC)}\right]\left[1 - \frac{0.7SN1}{SN_1+\exp(-5.51+22.9SN1)}\right] \tag{5}$$

where SAN is the sand content (%); SIL is the silt content (%); CLA is the clay content (%); OC is the soil organic carbon content (%); and $SN_1 = 1 - SAN/100$.

(3) Topographic factor (LS)

The LS factor represents the topographic characteristics that influence water erosion. It was calculated using the Desmet and Govers (1996) method in SAGA-GIS (Automated Geoscience Analysis System).

$$LS = (m+1)\left(\frac{U}{L_0}\right)^{m}\left(\frac{\sin\theta}{S_0}\right)^{n} \tag{6}$$

where U is the area contributing to upslope per unit width ($m^2 \cdot m^{-1}$); θ is the slope derived from DEM; L_0 is the standard plot's length (22.1 m); S_0 is the standard plot's slope (0.09); and m and n are dependent on the main erosion types ($m = 0.4$–0.6 and $n = 1.0$–1.3), and default empirical values in SAGA-GIS were used for m and n. The m and n values are based on the default values in SAGA-GIS.

(4) Cover management factor (C)

The C factor reflects the ability of vegetation to inhibit soil erosion. It was calculated by FVC as follows (Cai et al.2000):

$$C = \begin{cases} 1 & 0 \\ 0.6508 - 0.3436 \times lg\,(FVC) & 0 < FVC < 78.3\% \\ 0 & FVC \geq 78.3\% \end{cases} \tag{7}$$

$$FVC = \frac{NDVI - NDVI_{soil}}{NDVI_{veg} - NDVI_{soil}} \tag{8}$$

where $NDVI$ is the normalized vegetation index;FVC is the vegetation coverage (%); $NDVI_{soil}$ represents the uncovered area's$NDVI$; and $NDVI_{veg}$ represents the$NDVI$ of the area covered by all vegetation.

(5) Conservation practice factor (P)

The P factor provides a comprehensive assessment of the impact of soil and water conservation measures on soil erosion. In this context, the regional distribution of P is primarily estimated using topography and land use types. The P factor of cultivated land was categorized by slope according to previous studies in the Loess Plateau region: 0°–5°, $P = 0.1$; 5°–10°, $P = 0.221$; 10°–15°, $P = 0.305$; 15°–20°, $P = 0.575$; 20°–25°, $P = 0.735$; >25°, $P = 0.80$ (Geng et al. 2022; Juan and Jing 2015; Xia et al. 2021). The P factors assigned to different land-use types were: grassland, $P = 1$; forest, $P = 1$; watershed, $P = 1$; urban, $P = 1$; bare land, $P = 1$ (Sun et al. 2014; Wischmeier and Smith 1978).

2.3.2 RWEQ Model

The wind erosion equation (WEQ) was initially developed by Woodruff and Siddoway (1965) as the first step in establishing a comprehensive theoretical system for understanding and predicting wind erosion. Over the years, considerable enhancements and refinements have been made to this equation, leading to the development of the revised wind erosion equation (RWEQ) by Fryrear et al. (2000). The RWEQ builds upon the foundation laid by the original WEQ and incorporates new insights and advancements in soil wind erosion research. Using the RWEQ, researchers can more accurately assess and quantify the potential for soil wind erosion in different environments. The equation, shown below, serves as a valuable tool in the study and management of soil wind erosion:

$$Q_{\max} = 109.8 \times (WF \times EF \times SCF \times K' \times C') \tag{9}$$

$$S = 150.71 \times (WF \times EF \times SCF \times K' \times C')^{-0.371} \tag{10}$$

$$S_L = \frac{2x}{S^2} Q_{max} e^{-\left(\frac{x}{S}\right)^2} \tag{11}$$

where Q_{max} is the maximum wind operation (kg·m^{-1}); S is the critical plot length (m); S_L is the soil loss (t·ha^{--1}·yr^{-1}); x is the maximum downwind wind erosion distance (m), taken as 50 m (Talukdar et al. 2022; Wang et al. 2023; Xing et al. 2021); WF is the weather factor (kg·m^{-1}); EF is the soil erodibility factor (unitless); C' is the vegetation cover factor (unitless); K' is the soil roughness factor (unitless); and SCF is the soil crust factor (unitless).

(1) Weather factor(WF).

WF is mainly related to wind speed, precipitation, evaporation, and irrigation. The formula is as follows:

$$WF = \frac{\sum_{i=1}^{N} U_2 (U_2 - U_t)^2 \times N_d \rho}{N \times g} \times SW \times SD \tag{12}$$

$$\rho = 348 \left(\frac{1.013 - 0.1183EL + 0.0048EL^2}{T} \right) \tag{13}$$

$$SW = \frac{ET_P - (R + I)\frac{R_d}{N_d}}{ET_P} \tag{14}$$

$$SD = 1 - P(\text{snow depth} > 25.4 \text{ mm}) \tag{15}$$

where U_2 is the wind speed at 2 m (m·s^{-1}), In this study, the wind speed at 10 m was converted to 2 m according to the wind profile (Elliot 1979).U_t is the critical wind speed at 2 m (m·s^{-1}), with 5 m·s^{-1} was used in this study; N_d is the number of days of observation (d); N is the total number of observations; ρ is the density of the air (kg·m^{-3}); g is the gravitational acceleration (m·s^{-2}), with 9.8 m·s^{-2} being used in this study; SW is the soil moisture coefficient (unitless);SD is the snow cover coefficient (unitless);EL is the elevation (km);T is the absolute temperature (K);ET_P is the potential relative evapotranspiration (mm);R is the 15-day rainfall amount (mm);I is the irrigation amount (mm), set to 0; R_d stands for rainfall days or irrigation days (d); N_d is the number of days of observation (d); and P stands for probability (snow depth exceeds 25.4 mm).

(2) Soil erosion factor (EF) and soil crust factor (SCF).

The SCF and EF factors are generally related to soil properties and calculated as follows:

$$EF = \frac{29.09 + 0.31SAN + 0.17Si}{100} + \frac{0.33(SAN/CLA) - 2.59OM - 0.95CaCO_3}{100} \tag{16}$$

$$SCF = \frac{1}{1 + 0.0066(CLA)^2 + 0.021(OM)^2} \tag{17}$$

where $CaCO_3$ is the calcium carbonate content (%), and OM is the organic matter content (%). In the absence of measured organic matter data, the organic matter content was estimated by multiplying the organic carbon content with the "Van Bemmelen factor" (Lin 2020).

(3) Surface roughness factor (K').

The surface roughness factor is mainly related to the terrain relief (Xu et al. 2019) and can be expressed as:

$$K' = e^{(1.86K_r - 2.41K_r^{0.934} - 0.127C_{rr})} \tag{18}$$

$$K_r = 0.2\frac{(\Delta H)^2}{L} \tag{19}$$

where K_r soil ridge roughness (cm); Crr is random roughness (cm); L is the topographic relief parameter; ΔH is the difference in elevation (m) within a range from L (Li et al. 2006).

(4) Vegetation cover factor (C').

Vegetation coverage directly affects near-surface wind speed, which in turn affects wind erosion intensity. It is calculated as follows (Wang et al. 2020; Xu et al. 2019):

$$C\prime = e^{-0.0438FVC} \tag{20}$$

where FVC is the vegetation coverage (%).

2.3.3 Trend Analysis Methods

The Mann–Kendall test is a nonparametric test, notable for not requiring the samples to follow a specific distribution and being immune to the influence of a few outliers. It is commonly used to assess the trends and significance of time series variations in elements such as precipitation, runoff, and temperature (Gao and Jin 2022; Güçlü 2018). In this study, the Mann-Kendall test was employed to determine the trends and significance of element changes over time. Additionally, the regression equation's slope was used to quantify the numerical value of the trend. The calculation formula is as follows (Li et al. 2018):

$$Slope = \frac{\sum_{i=1}^{n} x_i t_i - \frac{1}{n}\left(\sum_{i=1}^{n} x_i\right)\left(\sum_{i=1}^{n} t_i\right)}{\sum_{i=1}^{n} (t_i)^2 - \frac{1}{n}\left(\sum_{i=1}^{n} t_i\right)^2} \quad (21)$$

where *Slope* is the trend of the variable *x*. If the *Slope* is greater than 0, *x* increases with increasing time *t*. If the slope is less than 0, *x* decreases with increasing time *t*.

3 Results

3.1 Analysis of Erosion Factors

3.1.1 Analysis of RUSLE Model Factors

(1) *R* factor

The *R* factor is an essential indicator of rainfall erosion capacity, which represents the extent of rainfall-induced soil erosion. It was calculated using Eqs. (2)–(4) as depicted in Fig. 2(a). Over multiple years, the average *R* factor in the study area was 2,449.63 $MJ{\cdot}mm{\cdot}ha^{-1}{\cdot}h^{-1}{\cdot}yr^{-1}$. The *R* factor exhibited significant spatial variation, with generally lower values in the western and northern parts and higher values in the eastern and southern parts. The *R* factors in different regions when ranked from largest to smallest were as follows: Valley Plain, Earth–rock Mountain, Gully, Hilly–gully, Sandy, and Irrigation regions. Overall, a comparison of the average *R* factor between the periods of 2000–2010 (2,304 $MJ{\cdot}mm{\cdot}ha^{-1}{\cdot}h^{-1}{\cdot}yr^{-1}$) and 2011–2021 (2,594.32 $MJ{\cdot}mm{\cdot}ha^{-1}{\cdot}h^{-1}{\cdot}yr^{-1}$) showed that the *R* factor exhibited an increasing trend over time, and this trend was observed in all regions.

(2) *LS* factor

The *LS* factor plays a critical role in comprehending the impact of slope length and steepness on soil erosion. We can identify suitable land management approaches to reduce soil erosion risks by calculating the *LS* factor. The *LS* factor was determined using Eq. (6), as shown in Fig. 2(b). The *LS* factor had an average value of 3.44, which indicates the overall topographic conditions that contribute to soil erosion. Notably, approximately 31.34% of the total area had *LS* values greater than or equal to the average value, which suggests that a considerable portion of the study area is relatively more susceptible to water erosion. Across different regions, the *LS* factor ranked highest in Gully regions, followed by Valley Plain, Earth–rock Mountain, Hilly–gully, Irrigation, and Sandy regions.

(3) *C* factor

The *C* factor represents the sensitivity of soil erosion based on different land types and cover conditions. Land managers must understand the importance and specific values of the *C* factor to develop effective land conservation and management strategies. In the case of the Loess Plateau, the *C* factor was calculated using Eqs. (7) and (8), as shown in Fig. 2(c). The *C* factor exhibited significant spatial and temporal variations across the Loess Plateau. Spatially, the western and northern parts generally had higher values, while the eastern and southern parts had lower values. In terms of temporal variation, statistical analysis of the average *C* factor during the periods of 2000–2010 (0.09) and 2011–2021 (0.07) revealed a decreasing trend in the *C* factor. In all regions, the *C* factor decreased over time. The *C* factor values in different regions when ranked from largest to smallest were as follows: Sandy, Irrigation, Gully, Hilly-gully, Valley Plain and Earth-rock Mountain regions.

(4) *K* factor

The *K* factor represents the erosion resistance of soil, which indicates how easily the soil can be eroded. A higher value of the *K* factor indicates a greater susceptibility to erosion. The *K* factor was calculated using Eq. (5), as illustrated in Fig. 2(d). Across the Loess Plateau, the *K* value ranged from 0.028 $t{\cdot}h{\cdot}MJ^{-1}{\cdot}mm^{-1}$ to 0.037 $t{\cdot}h{\cdot}MJ^{-1}{\cdot}mm^{-1}$. The regional average value was 0.033 $t{\cdot}h{\cdot}MJ^{-1}{\cdot}mm^{-1}$, with a gradual increase observed from north to south throughout the area. The *K* factor values decreased in the following order: Gully, Valley Plain, Earth–rock Mountain, Irrigation, Hilly–gully, and Sandy regions.

(5) *P* factor

The *P* factor, which is an indicator of the effectiveness of soil erosion control, generally remained stable across the Loess Plateau from the year 2000 to 2021. Low *P* factor values indicate good soil conservation. The *P* factors in different regions when ranked from largest to smallest were as follows: Sandy, Hilly–gully, Gully, Earth–rock Mountain, Irrigation, and Valley Plain regions.

3.1.2 Analysis of RWEQ Model Factors

(1) Weather factor (*WF*)

The weather factor (*WF*) reflects the combined effect of multiple weather factors, including wind speed,

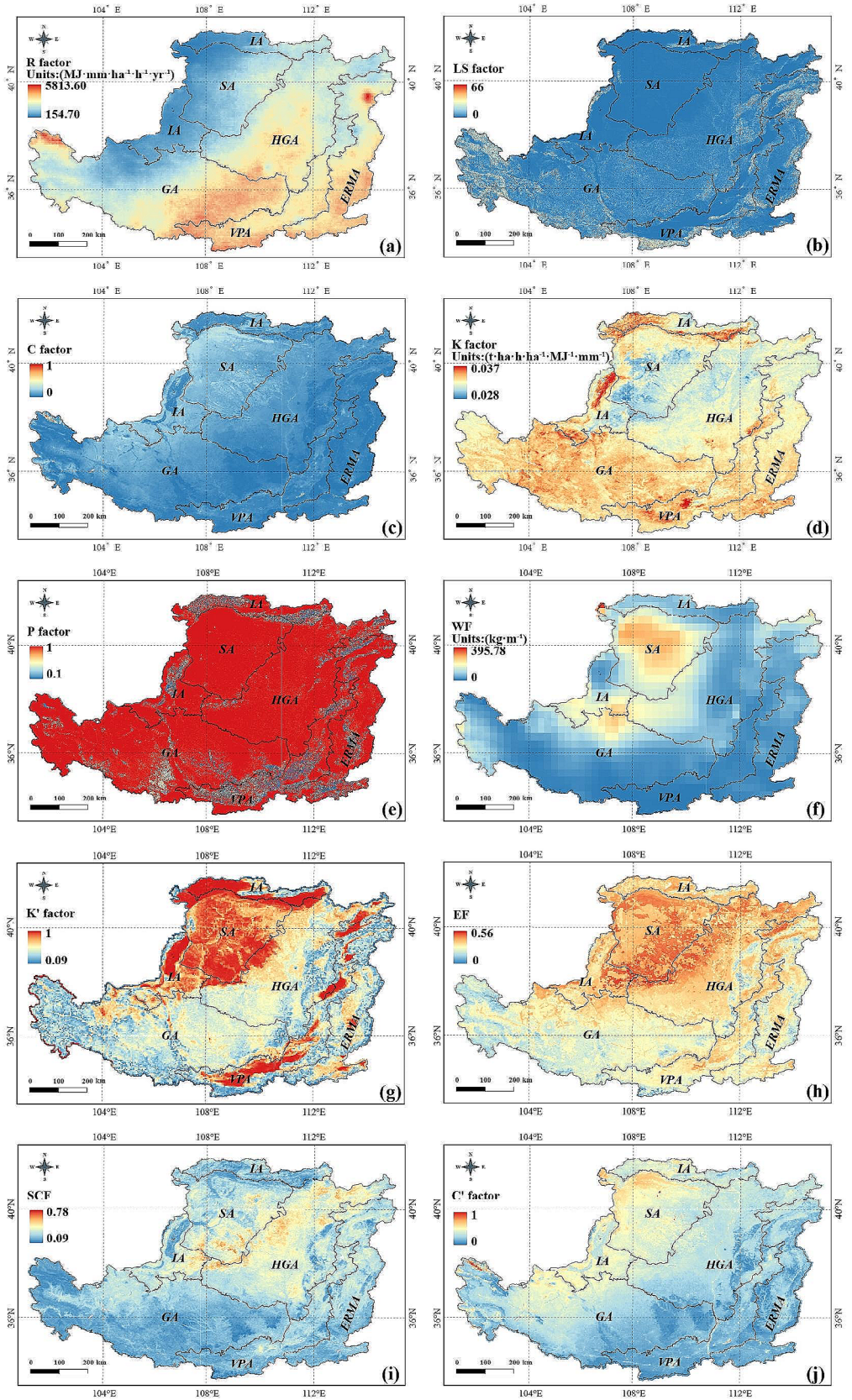

Fig. 2 Spatial distribution characteristics of average erosion factors from the year 2000 to 2021. (**a**)–(**e**) represents the *R*, *LS*, *C*, *K*, and *P* factors of the RUSLE model, and (**f**)–(**j**) represents the *WF*, *K'*, *EF*, *SCF* and *C'* factors of the RWEQ model, respectively

precipitation, temperature, and snow cover factor, on soil wind erosion. A high *WF* value, indicates a high risk of wind erosion. *WF* was calculated using Eqs. (12)–(15), as illustrated in Fig. 2(f). The calculation of the average values of *WF* for the periods of 2000–2010 (75.96 $kg \cdot m^{-1}$) and 2011–2021 (82.29 $kg \cdot m^{-1}$) reveals a certain increase in *WF*. In addition, *WF* exhibited significant spatial variation, with high-value areas mainly distributed in the northwest and west-central regions. The *WF* values among different regions when ranked from highest to lowest were as follows: Gully, Valley plain, Earth–rock Mountain, Irrigation, Sandy, Hilly–gully regions. Notably, the *WF* values in the Gully and Earth–rock Mountain regions showed a decreasing trend over time, while those in other regions all showed an increasing trend.

(2) *K'* factor

The *K'* factor reflects the influence of land surface roughness on soil wind erosion. The *K'* factor, which was calculated using Eqs. (18) and (19), is presented in Fig. 2(g). Spatially, the surface roughness factor was larger in the northwest and southeast regions of the Loess Plateau and smaller in other regions. The *K'* factor values among different regions when ranked from highest to lowest were as follows: Gully, Sandy, Irrigation, Valley Plain, Hilly–gully and Earth–rock Mountain regions.

(3) Soil erodibility factor (*EF*) and soil crust factor (*SCF*)

The soil erodibility factor (*EF*) and soil crust factor (*SCF*) collectively assess the vulnerability of soil to wind erosion. *EF*, which was calculated using Eq. (0) and is visualized in Fig. 2(h), quantifies the inherent susceptibility of soil based on its physical, chemical, and mechanical properties. Meanwhile, *SCF*, which was calculated using Eq. (17) and is visualized in Fig. 2(i), reflects the protective effect of a hardened crust on the soil surface. Spatially, *EF* exhibited a decreasing trend from northwest to southeast, while *SCF* showed higher values in the north-central region than in other areas. When examining different regions, *EF* ranked highest in the Sandy region and lowest in the Gully region, with those in Irrigation, Hilly–gully, Earth–rock Mountain, and Valley Plain regions falling in between. Similarly, *SCF* ranked highest in the Hilly–gully region and lowest in the Gully region, following the same order for the other regions as *EF*.

(4) *C'* factor

The *C'* factor, which was calculated using Eq. (20) and is displayed in Fig. 2(j), quantifies the extent to which vegetation cover suppresses soil wind erosion, with low values indicating great suppression. Over time, the *C'* factor on the Loess Plateau has shown a significant downward trend statistically (with an average of 0.30 for the period 2000–2010 and 0.27 for the period 2011–2021), which indicates a decline in the protective capacity of vegetation. Spatially, the *C'* factor increased from southeast to northwest, which implies a high level of vegetation protection in the northwestern region. In all regions, the *C'* factor showed a statistically significant decreasing trend over time. The *C'* factor values in different regions when ranked from highest to lowest, were as follows: Sandy, Irrigation, Hilly–gully, Gully, Earth–rock Mountain, and Valley Plain.

3.2 Spatiotemporal Characteristics of Soil Erosion

3.2.1 Spatial Distribution Characteristics

(1) Water erosion

The average multiannual water erosion rate in the Loess Plateau region was 14.56 $t \cdot ha^{-1} \cdot yr^{-1}$, which decreased overall over time. The average erosion intensity was 16.48 $t \cdot ha^{-1} \cdot yr^{-1}$ from the year 2000 to 2010, and it was 12.64 $t \cdot ha^{-1} \cdot yr^{-1}$ from the year 2010 to 2021 (Fig. 3(a) and 3(b)). In the year 2020, the erosion intensity reached its minimum at 7.46 $t \cdot ha^{-1} \cdot yr^{-1}$. Spatially, high water erosion rates were observed in the northeast, southwest, and central regions, while low rates were found in the northwest and southeast. All subregions showed a decreasing trend in water erosion rates. The Gully region had the highest erosion rate at 28.95 $t \cdot ha^{-1} \cdot yr^{-1}$ over the multiyear period, while the sandy region had the lowest erosion rate at 2.23 $t \cdot ha^{-1} \cdot yr^{-1}$. The other subregions, which were ranked by decreasing water erosion rate, were the Valley Plain region, Hilly–gully region, Earth–rock Mountain region, and Irrigation region, with multiyear average water erosion rates of 11.83, 10.53, 8.15, and 6.56 $t \cdot ha^{-1} \cdot yr^{-1}$, respectively.

(2) Wind erosion

The average wind erosion rate in the study area has been 3.95 $t \cdot ha^{-1} \cdot yr^{-1}$ over the years. The temporal variation of wind erosion rate differs from that of water erosion. According to the available data, the average wind erosion rate during 2000–2010 was 3.73 $t \cdot ha^{-1} \cdot yr^{-1}$, while it increased to 4.16 $t \cdot ha^{-1} \cdot yr^{-1}$ during 2011–2021, which indicates a slightly increasing trend (Fig. 3(c) and (d)). Notably, wind erosion mainly occurred in the Sandy region, which affected only small areas of the Irrigation and Hilly–gully regions. In addition, wind erosion was seldom observed in the Valley Plain, Earth–rock Mountain, and Gully regions, which suggests the existence of effective natural barriers or land characteristics that restrict wind erosion in those areas.

3.2.2 Temporal Characteristics of Soil Erosion

(1) Erosion power source

Water and wind erosion occur due to specific rainfall intensity or wind speed. In this study, the erosive rainfall and wind speed were calculated every half-month for the

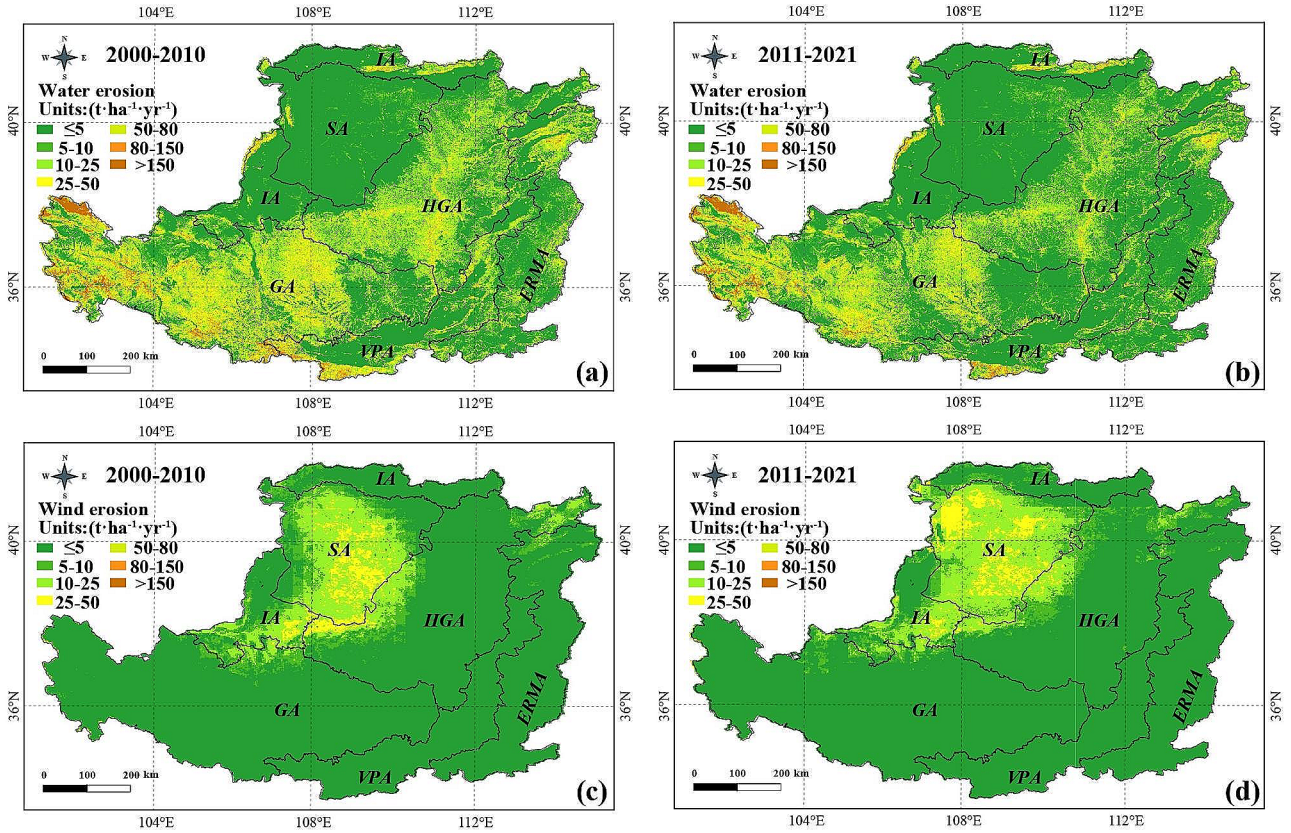

Fig. 3 Spatial variation patterns of soil erosion on the Loess Plateau from 2000–2010 and 2011–2021. (**a**) and (**b**) depict the spatial variation pattern of water erosion from 2000–2010 and 2011–2021, respectively; (**c**) and (**d**) illustrate the spatial variation pattern of wind erosion from 2000–2010 and 2011–2021, respectively

entire area from the year 2000 to 2021. The results are shown in Figs. 4 and 5. Daily rainfall (> 12 mm) and wind speed (> 5 $m \cdot s^{-1}$) were analyzed using GEE. The maximum erosive rainfall, which was recorded at 99.29 mm, was observed in July of 2013, specifically the first half of the month. Meanwhile, certain months had no erosive rainfall in some years. The highest erosive wind speed, which was measured at 7.15 $m \cdot s^{-1}$, occurred in the first half of March 2001. By contrast, the lowest speed, which was measured at 5.36 $m \cdot s^{-1}$, was recorded in the second half of February 2019. Erosive rainfall and wind speed exhibited notable fluctuations within a year and between years. Most erosive rainfall occurred during the summer months (June, July, and August). Meanwhile, most erosive wind occurred during the spring months (March, April, and May). Consequently, protecting against water erosion during summer and from wind erosion during spring is crucial.

Erosive rainfall and wind speed exhibited increasing trends in magnitude over the years, with respective increasing rates of + 4.59 mm per year ($p < 0.05$) and + 0.009 $m \cdot s^{-1}$ per year ($p < 0.05$). In terms of occurrence frequency, erosive rainfall showed an increasing trend of 0.05% per year ($p < 0.05$), while erosive wind exhibited no significant trend ($p > 0.05$). These results indicate that the intensity and frequency of erosive rainfall are increasing, while the intensity of erosive wind is increasing; however, its frequency shows considerable fluctuations.

(2) Erosion intensity

Figure 6 presents the temporal variation characteristics of water and wind erosion. The average change rates for wind and water erosion in the area were 0.035 ($p > 0.05$) and − 0.461 ($p < 0.05$) $t \cdot ha^{-1} \cdot yr^{-1} \cdot yr^{-1}$, respectively. This finding indicates a significant decreasing trend in water erosion over time, but no significant trend in wind erosion over time. Wind erosion exhibited greater temporal variability than water erosion, which is primarily due to extreme weather events. For example, wind erosion in the Loess Plateau experienced significant fluctuations in 2021. According to statistics, the frequency and magnitude of wind erosion in 2021 increased by 31.63% and 2.66%, respectively, compared with those in 2020. Moreover, the erosion rate surged by 184.40% in 2021, which marked the highest value during the study period. By contrast, water erosion demonstrated a

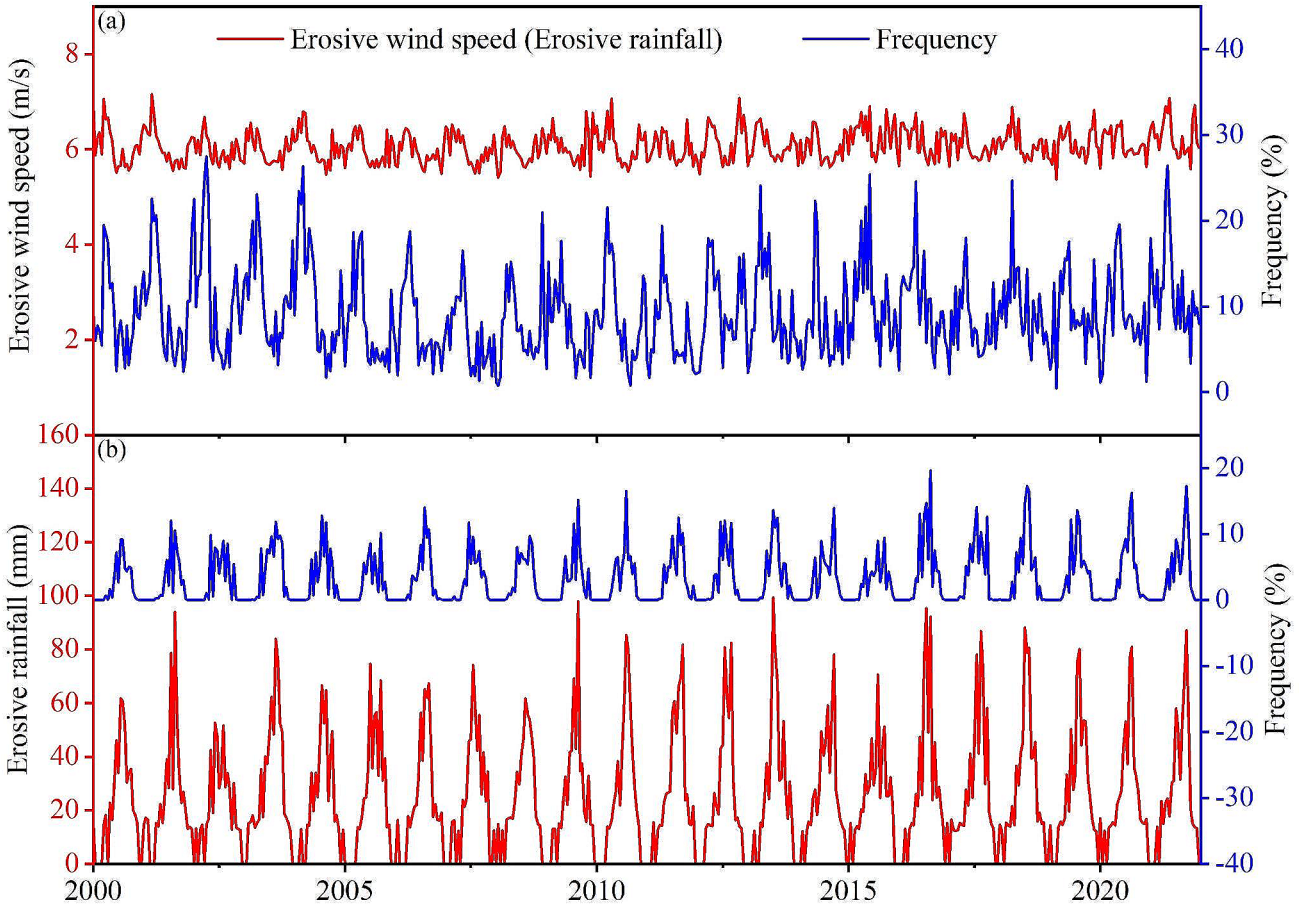

Fig. 4 Semimonthly temporal variation characteristics of erosive rainfall and erosive wind on the Loess Plateau. (**a**) and (**b**) represent erosive wind and rainfall, respectively

significant trend over time, with the trend indicated by its slope being more persuasive than that of wind erosion.

3.3 Erosion Classification

(1) Water erosion classification

In this study, soil erosion was classified into the following six levels: very slight (<5 t·ha^{-1}·yr^{-1}), slight (5–10 t·ha^{-1}·yr^{-1}), light (10–25 t·ha^{-1}·yr^{-1}), moderate (25–50 t·ha^{-1}·yr^{-1}), severe (50–80 t·ha^{-1}·yr^{-1}), very severe (80–150 t·ha^{-1}·yr^{-1}), and extremely severe (>150 t·ha^{-1}·yr^{-1}). The erosion classes of water and wind erosion are shown in Table 2. From the year 2000 to 2005, the average percentage of the very slight water erosion class was 47.32%, which increased to 60.05% from the year 2016 to 2021. The area with a slight water erosion class tended to increase over time, while the proportion with a light water erosion class tended to decrease. A small proportion of erosion was also classified as extremely severe, very severe, severe, and moderate. On average, these classes accounted for less than 10% of the studied years, and their proportion decreased over time, which reflects the overall decreasing trend in erosion across the Loess Plateau.

Among the six subregions, the Sandy region had a higher proportion of very slight water erosion than the other subregions. From the year 2000 to 2021, more than 80% of the area in the Sandy region showed very slight erosion, which indicates a low erosion intensity. Meanwhile, the Gully region had the lowest proportion of areas with very slight water erosion, which averaged 32.82% from the year 2000 to 2021. This observation reflects a high erosion rate in that area. Over time, an increasing trend was observed in the proportion of areas with very slight and slight water erosion, while other erosion classes showed a decreasing trend. This observation suggests that the rate of water erosion has generally decreased in the entire area.

(2) Wind erosion classification

The proportion of areas classified as having very slight wind erosion in the entire region showed a trend of increasing first and then decreasing, with a slight overall decrease and considerable volatility. Among all the subregions, the Sandy region on the Loess Plateau experienced the most

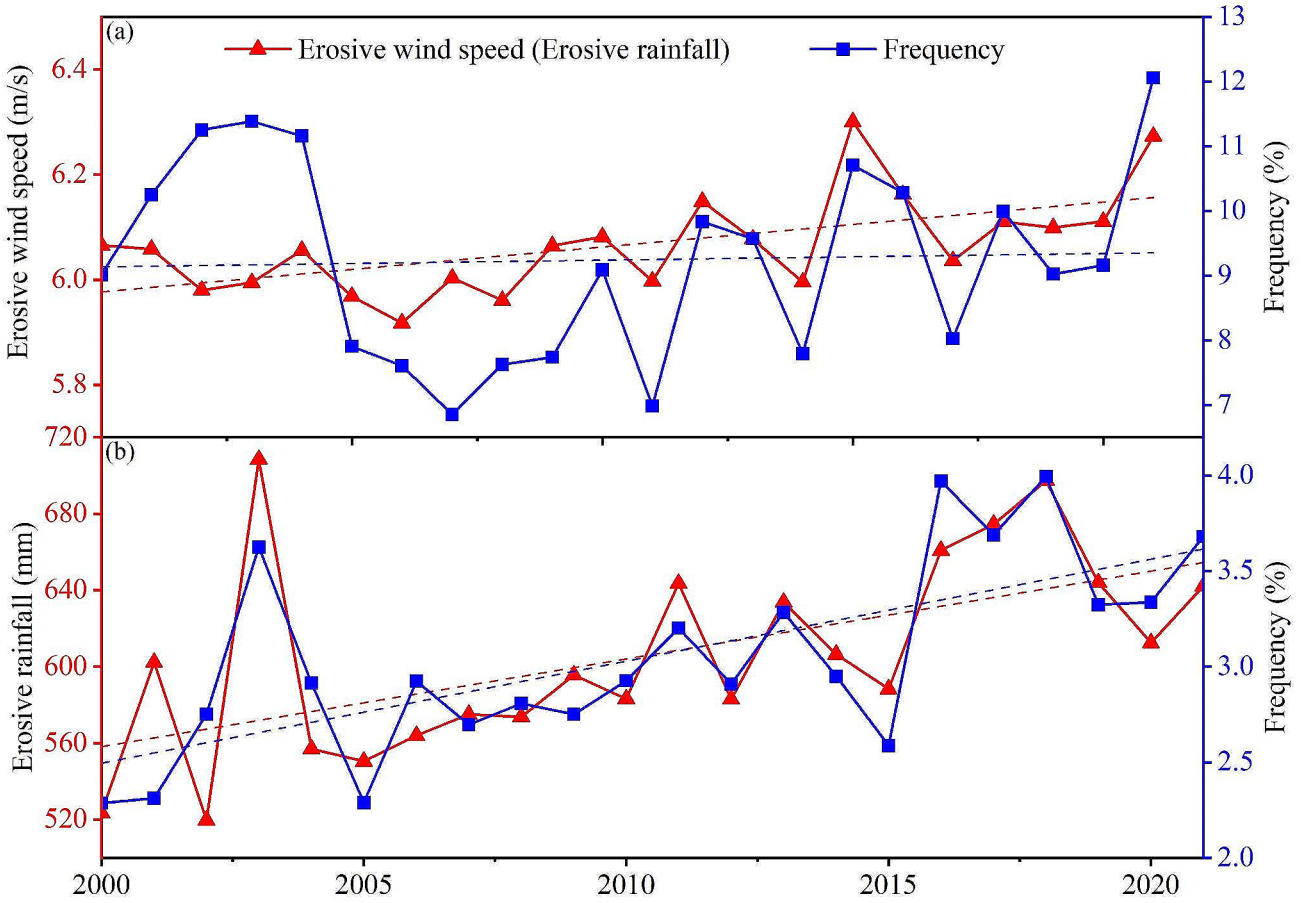

Fig. 5 Annual temporal variation characteristics of erosive rainfall and erosive wind on the Loess Plateau. (**a**) and (**b**) represent erosive wind and rainfall, respectively

severe wind erosion. Only 17.33% (multiyear average) of the area in this region was categorized as having very slight wind erosion. By contrast, all other areas, except for the Sandy region, were mainly classified as having very slight wind erosion. The Earth–rock Mountain, Gully, and Valley Plain regions had about 95% areal percentage with a very slight wind erosion classification.

3.4 Model Validation

3.4.1 Water Erosion Model Verification

Currently, the accuracy of model simulations is generally verified by comparing them with measured data or simulation results from other scholars (Chen and PF, 2019; Geng et al. 2022; Guo and Shao 2019). However, measured data are difficult to obtain on a large scale, and the spatial resolution of the sampling area is often inconsistent with the simulation results. Therefore, this study used publicly available research data from the same study area to verify the simulation accuracy (Table 3). The results showed that the relative error between this study and the relevant research results was between − 0.42 and 0.79, which indicates a good overall simulation accuracy.

3.4.2 Wind Erosion Model Verification

The intensity of wind erosion is often used as an indicator of the frequency and intensity of sandstorms. Therefore, many scholars have assessed the accuracy of simulation results by comparing the intensity of wind erosion with the frequency of sandstorms (Lin et al. 2021b; Zhang et al. 2019). In this study, the frequency of sandstorms in the area from the year 2000 to 2007 was statistically analyzed using sandstorm data from weather stations in the region to validate the simulated wind erosion intensity. From an interannual variation perspective, the changes in sandstorm frequency and wind erosion intensity exhibited remarkable consistency. A strong positive correlation existed between wind erosion intensity and sandstorm frequency in the Loess Plateau. Furthermore, a significant positive correlation existed between wind erosion intensity and sandstorm frequency in each subregion

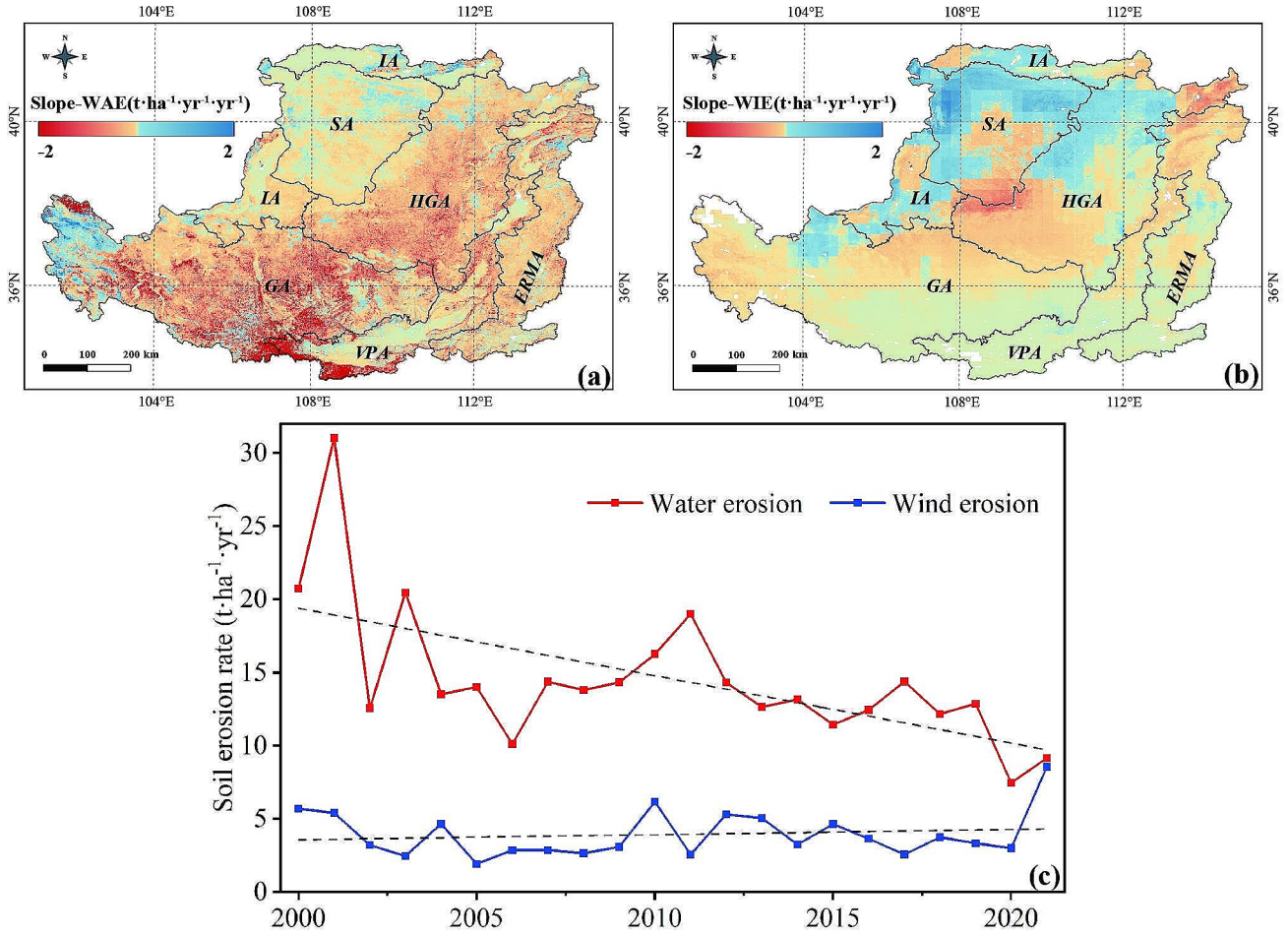

Fig. 6 Temporal variation of water and wind erosion on the Loess Plateau. WAT is the water erosion trend, and WIT is the wind erosion trend. (**a**) and (**b**) are the spatial distribution patterns of the *Slope* from 2000 to 2021, and (**c**) is the changing trend of average water and wind erosion from 2000 to 2021

Table 2 Proportion of erosion classes on the Loess Plateau from the year 2000 to 2021

Soil erosion class	2000–2005		2006–2010		2011–2015		2016–2021	
	WAE	WIE	WAE	WIE	WAE	WIE	WAE	WIE
Very slight	47.32%	78.45%	53.83%	82.04%	53.26%	78.38%	60.05%	77.93%
Slight	14.59%	8.20%	15.99%	5.46%	16.11%	6.25%	15.16%	7.42%
Light	20.40%	9.94%	18.61%	8.85%	18.76%	10.83%	15.57%	10.73%
Moderate	10.39%	3.25%	7.30%	3.51%	7.47%	4.47%	5.80%	3.42%
Severe	3.73%	0.16%	2.21%	0.14%	2.27%	0.07%	1.76%	0.50%
Very severe	2.24%	0%	1.25%	0%	1.30%	0%	1.01%	0%
Extremely severe	1.33%	0%	0.81%	0%	0.83%	0%	0.65%	0%

Note: WAE and WIE represent water erosion and wind erosion, respectively

Table 3 Comparison of water erosion simulation results with other studies

Reference	Region	Period	Method	Reference research	Current research	Relative error
(Sun et al. 2014)	Loess Plateau, China	2000–2010	RUSLE	15.20	16.48	0.08
(Guo and Shao 2019)	Loess Plateau, China	2000–2015	RUSLE	20.89	15.74	-0.25
(Fu et al. 2011)	Loess Plateau, China	2000 (2008)	RUSLE	33.57 (23.99)	20.73 (13.81)	-0.38 (-0.42)
(Gao et al. 2016)	Loess Plateau, China	2010	RUSLE	19.21	16.26	-0.15
(Lin et al. 2021a)	Loess Plateau, China	2000(2020)	RUSLE	5.03 (11.61)	20.73 (7.46)	0.79 (0.48)

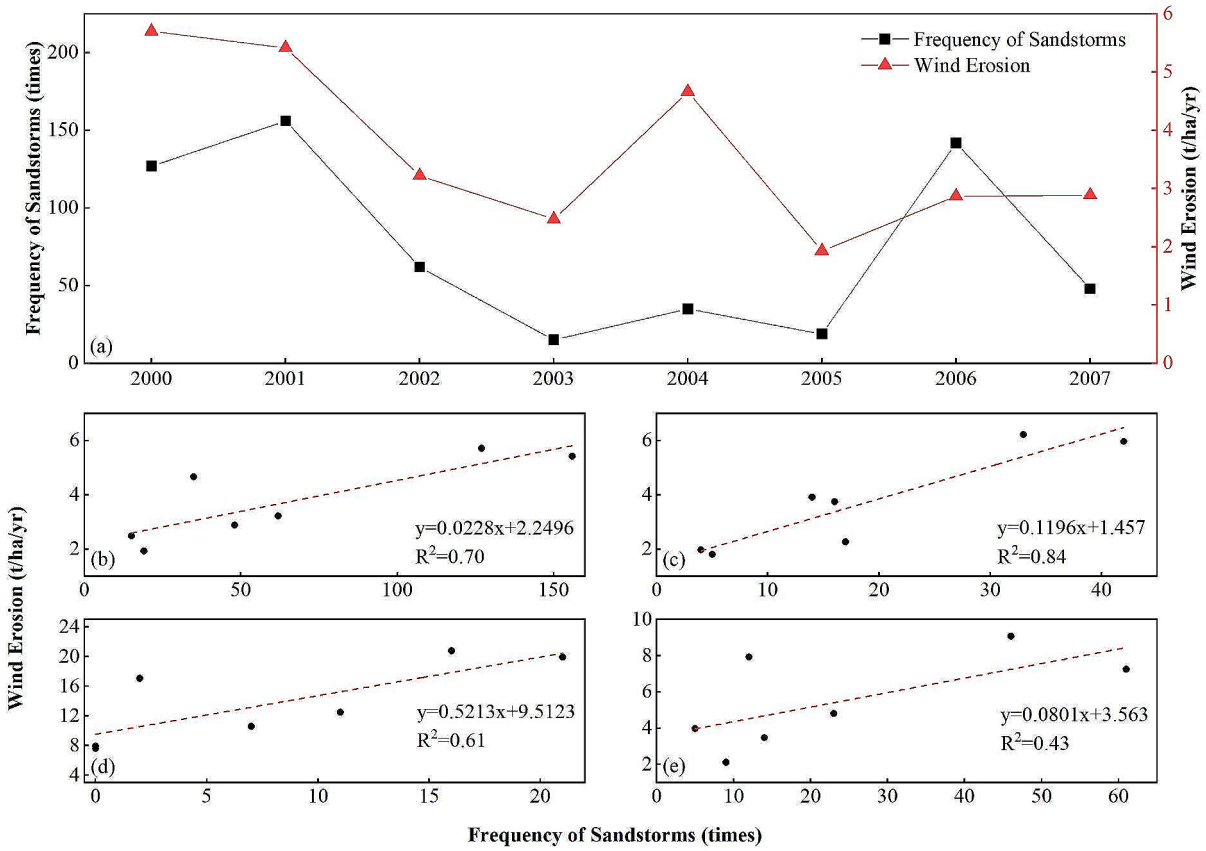

Fig. 7 Correlation between wind erosion intensity and sandstorm frequency. (**a**) displays the interannual variation of wind erosion intensity and sandstorm frequency; (**b**)–(**e**) represent the correlation for different regions: total Loess Plateau, Hilly-gully region, Sandy region, and Irrigation region, respectively

Table 4 Characteristics of changes in land use types

Land use	2000–2005	2006–2010	2011–2015	2016–2021	2000–2021
	Percentage(%)	Percentage(%)	Percentage(%)	Percentage(%)	Percentage(%)
Cropland	25.46	24.73	23.86	24.62	24.67
Forest	13.82	14.14	14.58	15.00	14.38
Grassland	42.73	44.16	44.66	45.42	44.24
Shrubland	10.15	9.34	9.31	7.47	9.07
Bare land	3.64	3.05	2.69	2.61	3.00
Others	4.20	4.58	4.90	4.88	4.64

(Fig. 7). Overall, the abovementioned results indicate that the simulation results are good.

4 Discussion

Rainfall and wind are crucial drivers of water and wind erosion, respectively, and play a vital role in the occurrence of soil erosion. The uncertainty and variability of meteorological factors, particularly the occurrence of extreme weather events, considerably influence the dynamic changes in soil erosion. According to the results in Sect. 3.2.2, erosive rainfall and wind speeds showed an increasing trend over the years, which led to further exacerbation of erosion. However, water erosion demonstrated a significant decreasing trend over time, while wind erosion exhibited no discernible trend, which implies that the changes in meteorological factors did not entirely dictate the direction of soil erosion trends. Since the implementation of the Grain for Green project, the areas of shrublands and bare lands have generally decreased, while forests and grasslands have increased. Moreover, the area of croplands initially decreased and then slightly increased, showing an overall declining trend (Table 4). The implementation of the Grain for Green project effectively improved the land-use structure (Tsunekawa et al. 2014). The primary direction of land-use transformation

is the conversion of croplands, bare lands, and shrublands into forests and grasslands. Furthermore, the vegetation coverage in the Loess Plateau has remarkably increased (Wang et al. 2021a; Zhang et al. 2020). Figure 8(a) shows the monthly average vegetation coverage in the entire region from the year 2000 to 2021. The research findings indicate that vegetation coverage has been increasing annually, albeit with seasonal variations. The average vegetation coverage was 29.20% in the year 2000, while it reached 34.65% in the year 2021, which exhibits an annual increase of 0.248% ($p < 0.05$). The optimization of land use types and the increase in vegetation coverage have effectively reduced the soil erosion risk caused by meteorological factors. Thus, the Loess Plateau now encounters a less intense and more challenges against soil erosion. This achievement reflects the remarkable effectiveness of the Grain for Green project. Overall, the role of the Grain for Green project in mitigating water erosion is more remarkable than that in wind erosion. For water erosion, it mainly occurs in summer and autumn. Vegetation coverage is relatively high at this time, providing increased resistance to erosive rainfall. On the one hand, wind erosion mainly occurs in the Sandy region of the northwest Loess Plateau. Drought and sparse rainfall in this region suppress vegetation growth, which results in minimal increases in vegetation coverage in recent years. On the other hand, wind erosion may predominantly occur in spring and winter when plants are either recently entering the growth period or in a dormant state. This situation results in low vegetation coverage on a large scale, which insufficiently exerts the inhibitory effect of vegetation on wind erosion.

A remarkable increase in vegetation cover has been observed on the Loess Plateau since the implementation of the Grain for Green project (Wang et al. 2021b; Zhang et al. 2020). Figure 8(a) shows the average monthly vegetation cover for the entire area from the year 2000 to 2021. During the said period, the highest vegetation cover was recorded in July (51.56%), August (53.53%), and September (46.79%). Vegetation cover plays a crucial role in mitigating wind and water erosion. From the year 2000 to 2021, vegetation cover substantially increased, effectively reducing the impacts of water and wind erosion. Figure 8(b) illustrates the spatial distribution of vegetation cover in 2021. Data revealed a clear trend of decreasing vegetation cover from the southeast to the northwest. The Valley Plain region exhibited the highest vegetation cover among the various subregions, which accounted for 49.76%. Close behind

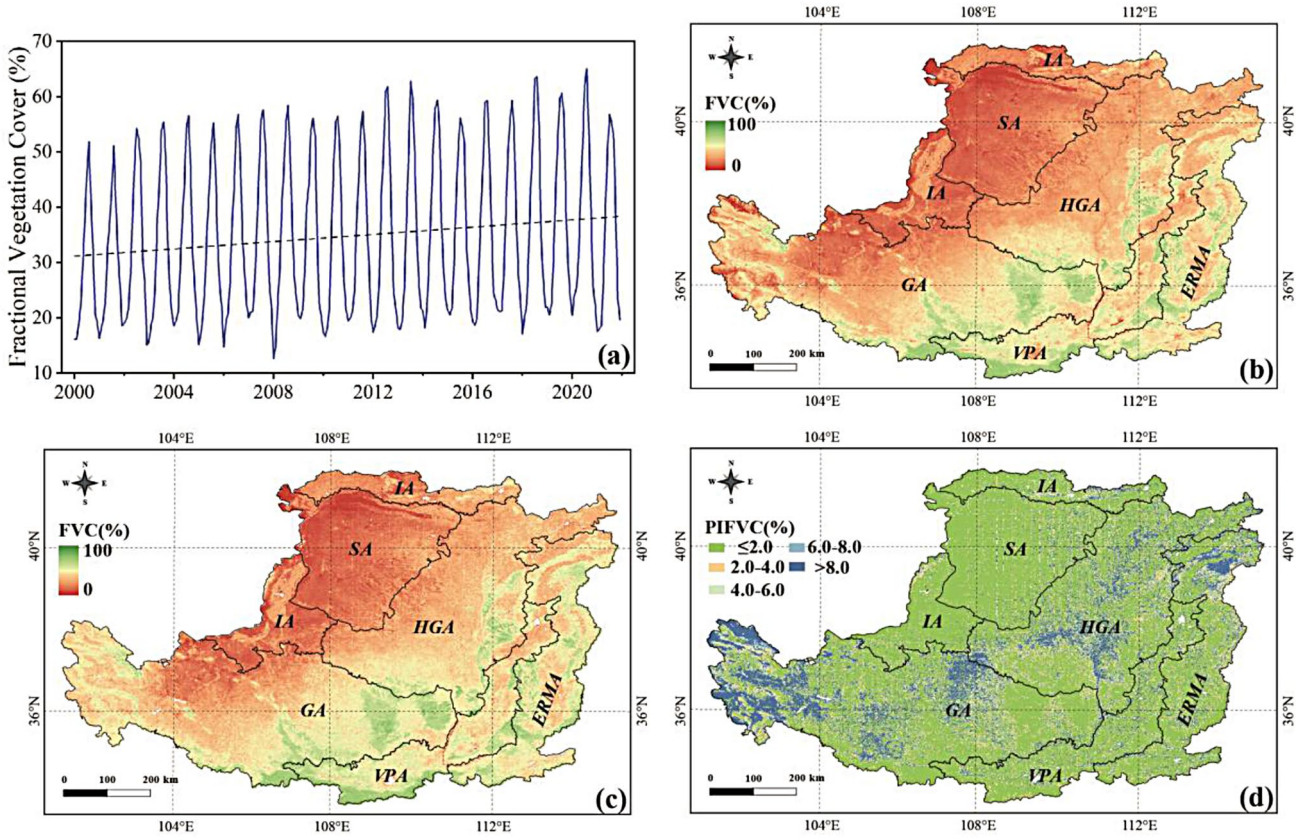

Fig. 8 Spatiotemporal characteristics of vegetation and management strategies for spatial layout. (**a**) shows the temporal variation characteristics of vegetation cover, (**b**) shows the vegetation cover distribution before vegetation improvement, (**c**) shows the vegetation cover distribution after vegetation improvement, and (**d**) shows the areas recommended for improvement

was the Earth–rock Mountain region, with a vegetation cover of 45.81%. The Gully, Hill–gully, Irrigation, and Sandy regions also contributed to the overall vegetation cover, with percentages of 37.88%, 34.77%, 20.21%, and 15.50%, respectively. These findings highlight the variability in vegetation cover across the study area and provide valuable insights into the distribution and abundance of vegetation in different regions.

While increasing vegetation can effectively control wind and water erosion, wind erosion primarily occurs in the Sandy region with low soil moisture and precipitation. In such areas, providing the necessary water for plant growth can be challenging (Meng et al. 2021). Therefore, this study focuses on improving vegetation cover in areas prone to water erosion. According to Wu et al. (2020), soil erosion approaches zero when vegetation cover exceeds 78.3%, and further increasing vegetation cover has no considerable effect. This study targets areas with vegetation cover below 78.3% and uses a mild water erosion risk threshold (5 $t \cdot ha^{-1} \cdot yr^{-1}$) for improving vegetation cover. Specifically, the required increase in vegetation cover to reduce the water erosion intensity from above the threshold to below the threshold was calculated. Figure 8(c) displays the enhanced vegetation coverage, while Fig. 8(d) illustrates the difference before and after the enhancement. According to Eq. (7), the enhancement scheme for vegetation coverage under the improvement target can be determined through reverse calculation. The average vegetation cover for the entire region should be 43.61%. Among the subregions, the vegetation coverage of the subregions should be as follows: Valley Plain region (51.95%), Earth-rock Mountain region (48.67%), Gully region (37.88%), Hilly-gully region (34.77%), Irrigation region (20.21%), and Sandy region (16.50%). The Gully region had the highest need for increased vegetation cover among all the sub-districts, which was measured at 4.29%. Meanwhile, the Sandy region had the lowest need for increased vegetation cover among the subdistricts, which was measured at 1.00%. The Hilly–gully region, Valley Plain region, Earth–rock Mountain region, and Irrigation region require an increase in vegetation cover of 3.27%, 2.18%, 2.86%, and 1.21%, respectively.

The increase in vegetation cover effectively suppresses soil erosion, but its effectiveness is limited. Therefore, the soil erosion conditions under the maximum potential vegetation cover needs to be explored to investigate further the development path of soil erosion on the Loess Plateau. Figure 9 illustrates the spatial distribution characteristics of water and wind erosion under current and target vegetation cover levels. The water erosion rate considerably decreased by 72.03% under the target vegetation cover, while the wind erosion rate decreased by only 7.20%. Across various regions, the order of decrease in water erosion rate was as follows: Gully region, Earth–rock Mountain region, Valley Plain region, Irrigation region, Hilly–gully region, and Sandy region. The order of decrease in wind erosion rate was as follows: Earth-rock Mountain region, Valley Plain region, Gully region, Hilly–gully region, Sandy region, and Irrigation region. Under ideal vegetation cover conditions, 18.50% of the areas experience water erosion classified as "very slight" or above, while 6.72% of the areas underwent wind erosion at the same classification. These regions are considered as areas where erosion cannot be solely mitigated by increasing vegetation cover. Thus, comprehensive soil and water conservation measures need to be implemented, including engineering solutions (such as on-land dams and sand dams) and agricultural practices (like optimizing planting structures and soil enhancement). However, regardless of the type of soil and water conservation measures adopted, they are not deemed as the most effective. Moreover, regardless of the type of soil and water conservation measures employed, their effectiveness in controlling soil erosion has certain limitations. Consequently, future soil erosion on the Loess Plateau will stabilize within a certain range in the region. Furthermore, management practices on the Loess Plateau influence the water and sediment inflow conditions of the Yellow River, which considerably affects its hydrological processes. In reality, less sediment in the Yellow River does not necessarily indicate improved conditions. A scarcity of sediment could lead to severe scouring downstream, which could result in distorted river formations and endanger flood control downstream. In addition, decreased sediment delivery at the Yellow River mouth and weaker sediment accumulation compared with seawater scouring slow down the rate of land formation or even cause a reduction in land formation areas. Thus, the management direction of the Loess Plateau should be aligned with the healthy development of the Yellow River Basin. In recent years, scholars have discussed the current status and development direction of the Loess Plateau and the Yellow River Basin from various perspectives. Jin et al. (2019) systematically analyzed the ecological governance process in the Loess Plateau, indicating a new stage in the ecological conditions of the region. Feng et al. (2016) suggested that the net primary productivity in the Loess Plateau is approaching its sustainable water resource limits. Hu et al. (2023) proposed regulating the sediment input into the Yellow River at approximately 300 million tons per year to balance soil erosion control and sediment transport in the main stream of the Yellow River. In general, the effectiveness of erosion control on the Loess Plateau will eventually have a limit from the perspective of objective capacity and actual needs.

In the modeling calculation, this study is based on substantial research on the regional soil and water conservation factor assessment methods in the Loess Plateau. Although the modeling needs can be achieved in general, the role of terraces cannot be fully considered. Further work can be based on remote sensing images through machine learning and field verification methods to derive the distribution of terraces over the years (Cao et al. 2020; Yu et al. 2022). This study back-calculates the appropriate target vegetation cover through the idea of

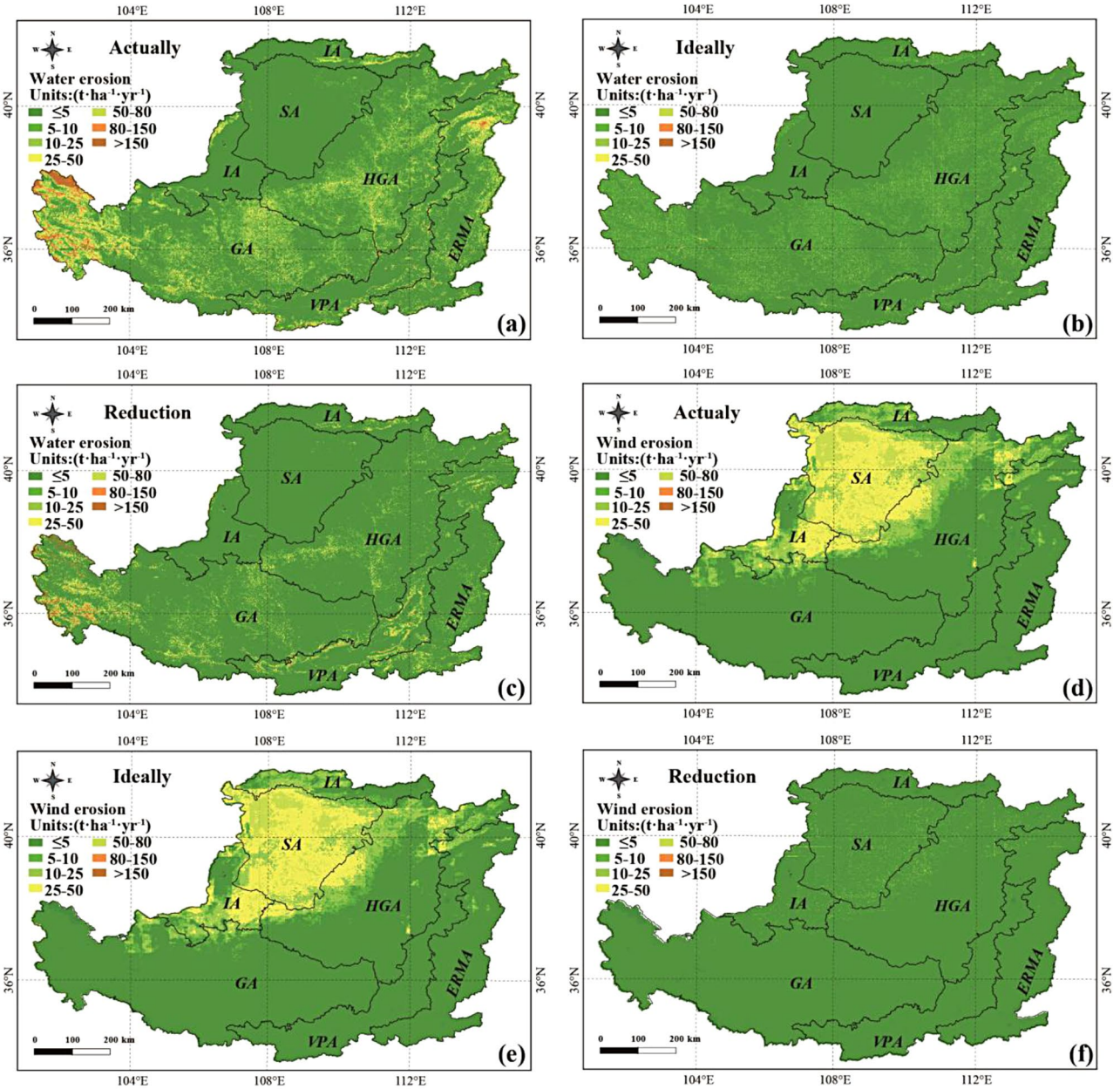

Fig. 9 Spatial distribution characteristics of water and wind erosion under current and target vegetation cover. (**a**) and (**d**) represent the spatial distribution of water erosion and wind erosion under current vegetation cover, respectively; (**b**) and (**e**) represent the spatial distribution of water erosion and wind erosion under ideal vegetation cover, respectively; (**c**) and (**f**) represent the difference between soil erosion under current vegetation cover and soil erosion under ideal vegetation cover

erosion degradation. Although the judgment is mainly based on the areas where water erosion occurs, which are generally not considered to be water scarce, the coordinated relationship between the restoration of vegetation cover and water supply capacity has not been directly discussed. The Loess Plateau and the Yellow River channel are a connected system. Many scholars have also recognized this point and have begun to coordinate the future healthy and stable development of the Loess Plateau and the Yellow River Basin from two aspects, namely, erosion control of the Loess Plateau and the hydrodynamic process of the Yellow River (Hu et al. 2022, 2023). In this study, we simulate the amount of erosion through the model, and the eroded sediment enters the Yellow River Basin channel after deposition as the Yellow River water and sand inlet conditions. However, the issues that need to be further explored are as follows: accurately quantifying the sediment deposition process at a large scale, predicting the accurate amount of sediment entering the Yellow River in different scenarios in the future, and

further investigating the quantitative indicators of the healthy development of the Loess Plateau–Yellow River system.

5 Conclusions

This study assessed the spatiotemporal characteristics of soil erosion in the Loess Plateau region from 2000 to 2021, evaluated the effectiveness of the "Grain for Green" project in mitigating water and soil loss, and proposed future directions for vegetation management in the Loess Plateau. Over the past two decades, there has been a noticeable decrease in water erosion intensity on the Loess Plateau, with an average intensity of 14.56 $t \cdot ha^{-1} \cdot yr^{-1}$, mainly concentrated within gully areas. In contrast, wind erosion intensity has shown a slight increase trend, with an average intensity of 3.95 $t \cdot ha^{-1} \cdot yr^{-1}$ primarily distributed in sandy regions. The "Grain for Green" project has significantly expanded grassland and forest areas, enhancing soil conservation capabilities and effectively mitigating water erosion. However, in arid and wind-prone regions, limited water resources challenge vegetation growth, hindering effective prevention of wind erosion. To enhance the efficacy of water and soil erosion control on the Loess Plateau, it is advisable to optimize vegetation coverage by increasing percentages in various regions: Gully region (4.29%), Hilly–gully region (3.27%), Valley Plain region (2.18%), Earth–rock Mountain region (2.86%), Irrigation region (1.21%), and Sandy region (1.00%).

Acknowledgements The National Natural Science Foundation of China (No. 52109064) and Open Research Fund of China Institute of Water Resources and Hydropower Research (YSS2022010) supported the research.

Declarations

Competing Interest The authors declare that they have no known competing financial interests or personal relationships that could have appeared to influence the work reported in this paper.

References

Cai CF, Ding SW, Shi ZH, Huang L, Zhang GY (2000) Study of applying USLE and geographical information system IDRISI to predict soil erosion in small watershed. J Soil Water Conserv 14:19–24

Cao B, Yu L, Naipal V, Ciais P, Li W, Zhao Y, Wei W, Chen D, Liu Z, Gong P (2020) A 30-meter terrace mapping in China using landsat 8 imagery and digital elevation model based on the Google Earth Engine. Earth Syst Sci Data Discuss 2020:1–35

Chen PF (2019) Monthly NPP dataset Covering China's terrestrial ecosystems at North of 18°N (1985–2015). J. Glob. Change Data Discov.

Chen L, Wei W, Fu B, Lü Y (2007) Soil and water conservation on the Loess Plateau in China: review and perspective. Prog Phys Geogr Earth Environ 31:389–403. https://doi.org/10.1177/0309133307081290

Desmet PJJ, Govers G (1996) A GIS procedure for automatically calculating the USLE LS factor on topographically complex landscape units. J Soil Water Conserv 51:427–433

Didan K (2021) MODIS/Terra Vegetation Indices 16-Day L3 global 1km SIN Grid V061. NASA EOSDIS land processes DAAC. 061. https://doi.org/10.5067/MODIS/MOD13A2. Accessed 2022-11-25 from

Elliot DL (1979) Adjustment and analysis of data for regional wind energy assessments, in: Workshop on Wind Climate, Asheville, North Carolina. pp. 121–31

Elnashar A, Zeng H, Wu B, Fenta AA, Nabil M, Duerler R (2021) Soil erosion assessment in the Blue Nile Basin driven by a novel RUSLE-GEE framework. Sci Total Environ 793:148466. https://doi.org/10.1016/j.scitotenv.2021.148466

Feng X, Fu B, Piao S, Wang S, Ciais P, Zeng Z, Lü Y, Zeng Y, Li Y, Jiang X (2016) Revegetation in China's Loess Plateau is approaching sustainable water resource limits. Nat Clim Change 6:1019–1022. https://doi.org/10.1038/nclimate3092

Fryrear DW, Bilbro JD, Saleh A, Schomberg H, Stout JE, Zobeck TM (2000) Improved wind erosion technology. J Soil Water Conserv 55:183–189

Fu B, Liu Y, Lü Y, He C, Zeng Y, Wu B (2011) Assessing the soil erosion control service of ecosystems change in the Loess Plateau of China. Ecol Complex 8:284–293. https://doi.org/10.1016/j.ecocom.2011.07.003

Funk C, Peterson P, Landsfeld M, Pedreros D, Verdin J, Shukla S, Husak G, Rowland J, Harrison L, Hoell A, Michaelsen J (2015) The climate hazards infrared precipitation with stations—a new environmental record for monitoring extremes. Sci Data 2:150066. https://doi.org/10.1038/sdata.2015.66

Gao H, Jin J (2022) Analysis of Water Yield Changes from 1981 to 2018 using an Improved Mann-Kendall Test. Remote Sens 14:2009. https://doi.org/10.3390/rs14092009

Gao H, Li Z, Jia L, Li P, Xu G, Ren Z, Pang G, Zhao B (2016) Capacity of soil loss control in the Loess Plateau based on soil erosion control degree. J Geogr Sci 26:457–472. https://doi.org/10.1007/s11442-016-1279-y

Geng WG, Zhu YQ, Chen PF (2022) 1-km Raster Dataset of Annual Soil Erosion Modulus on the Loess Plateau (2001–2015)[J]. J. Glob. Change Data Discov. 1, 85–92

Gorelick N, Hancher M, Dixon M, Ilyushchenko S, Thau D, Moore R (2017) Google Earth Engine: planetary-scale geospatial analysis for everyone. Remote Sens Environ 202:18–27. https://doi.org/10.1016/j.rse.2017.06.031

Güçlü YS (2018) Multiple Şen-innovative trend analyses and partial Mann-Kendall test. J Hydrol 566:685–704. https://doi.org/10.1016/j.jhydrol.2018.09.034

Guo X, Shao Q (2019) Spatial pattern of Soil Erosion drivers and the Contribution rate of human activities on the Loess Plateau from 2000 to 2015: a Boundary line from Northeast to Southwest. Remote Sens 11:2429. https://doi.org/10.3390/rs11202429

Guo Q, Ding Z, Qin W, Cao W, Wen W, Xu X, Yin Z (2019) Changes in sediment load in a typical watershed in the tableland and gully region of the Loess Plateau, China. CATENA 182:104132. https://doi.org/10.1016/j.catena.2019.104132

Hu CH, Zhang S, Zhang X (2022) Research on water and sediment regulation of the Yellow River under new situation. J Strateg Study CAE 24:122–130. https://doi.org/10.15302/J-SSCAE-2022.01.013

Hu C, Zhang Z, Zhang X (2023) Threshold system of regulation indicators for maintaining the runoff and sediment balance ofthe Yellow River basin. Adv Water Sci 34:647–659. https://doi.org/10.14042/j.cnki.32.1309.2023.05.001

Jin Z (2019) Ecological restoration and ecological governance of the Loess Plateau in a new era. J Earth Environ 10:316–322

Juan W, Jing Z (2015) Quantitative Assessment of Soil Erosion in Areas under Grain for Green Project in Loess Plateau of Northern Shaanxi Province based on GIS and RS. Bull. Soil Water Conserv

Li J, You SC, Huang JF (2006) Spatial distribution of ground roughness length based on GIS in China. J Shanghai Jiaotong Univ Agric Sci 24:185–189

Li D, Xu D, Wang Z, You X, Zhang X, Song A (2018) The dynamics of sand-stabilization services in Inner Mongolia, China from 1981 to 2010 and its relationship with climate change and human activities. Ecol Indic 88:351–360. https://doi.org/10.1016/j.ecolind.2018.01.018

Li J, Liu Q, Feng X, Shi W, Fu B, Lü Y, Liu Y (2019) The synergistic effects of afforestation and the construction of check-dams on sediment trapping: four decades of evolution on the Loess Plateau, China. Land Degrad Dev 30:622–635. https://doi.org/10.1002/ldr.3248

Li X, Luo J, Jin X, He Q, Niu Y (2020) Improving Soil Thickness estimations based on multiple environmental variables with stacking ensemble methods. Remote Sens 12:3609. https://doi.org/10.3390/rs12213609

Lin J (2020) Spatiotemporal pattern and driving factors of Soil Erosion in Hexi Region. Lanzhou University Lanzhou, China

Lin J, Guan Q, Pan N, Zhao R, Yang L, Xu C (2021a) Spatiotemporal variations and driving factors of the potential wind erosion rate in the Hexi region, PR China. Land Degrad Dev 32:139–157. https://doi.org/10.1002/ldr.3702

Lin J, Guan Q, Pan N, Zhao R, Yang L, Xu C (2021b) Spatiotemporal variations and driving factors of the potential wind erosion rate in the Hexi region, PR China. Land Degrad Dev 32:139–157. https://doi.org/10.1002/ldr.3702

Meng X, Cao J, Wang X (2021) Analysis of soil erosion in central and eastern China: a spatial model approach. J Soil Water Conserv 76:276–290. https://doi.org/10.2489/jswc.2021.00088

Mu X, Li P, Liu B, Zhao G, Gao P, Sun W (2022) Spatial-temporal development and driving mechanisms of Erosion on the Chinese Loess Plateau between 1901 and 2016. Yellow River 44:36–45

Muñoz Sabater J (2019) ERA5-Land hourly data from 2001 to present. https://doi.org/10.24381/CDS.E2161BAC

Nachtergaele F, Velthuizen HV, Verelst L, Wiberg D (2009) Harmonized World Soil Database (HWSD). Food Agric. Organ. U. N. Rome

Poggio L, De Sousa LM, Batjes NH, Heuvelink G, Kempen B, Ribeiro E, Rossiter D (2021) SoilGrids 2.0: producing soil information for the globe with quantified spatial uncertainty. Soil 7:217–240. https://doi.org/10.5194/soil-7-217-2021

Shi H, Shao M (2000) Soil and water loss from the Loess Plateau in China. J Arid Environ 45:9–20. https://doi.org/10.1006/jare.1999.0618

Sun W, Shao Q, Liu J, Zhai J (2014) Assessing the effects of land use and topography on soil erosion on the Loess Plateau in China. CATENA 121:151–163. https://doi.org/10.1016/j.catena.2014.05.009

Talukdar I, Kowal V, Huang B, Weil C (2022) Vegetation Drastically Reduces Wind Erosion: An Implementation of the RWEQ in the Mongolian Gobi Steppe. Land 11, 1204. https://doi.org/10.3390/land11081204

Tsunekawa A, Liu G, Yamanaka N, Du S (2014) Restoration and development of the degraded Loess Plateau, China. Springer

Wang W, Samat A, Ge Y, Ma L, Tuheti A, Zou S, Abuduwaili J (2020) Quantitative soil wind Erosion potential mapping for Central Asia using the Google Earth Engine platform. Remote Sens 12:3430. https://doi.org/10.3390/rs12203430

Wang J, Liu Z, Gao J, Emanuele L, Ren Y, Shao M, Wei X (2021a) The grain for Green project eliminated the effect of soil erosion on organic carbon on China's Loess Plateau between 1980 and 2008. Agric Ecosyst Environ 322:107636. https://doi.org/10.1016/j.agee.2021.107636

Wang J, Liu Z, Gao J, Emanuele L, Ren Y, Shao M, Wei X (2021b) The grain for Green project eliminated the effect of soil erosion on organic carbon on China's Loess Plateau between 1980 and 2008. Agric Ecosyst Environ 322:107636. https://doi.org/10.1016/j.agee.2021.107636

Wang L, Zhao X, Zhang C, Tang W (2023) Assessment of windbreak and sand fixation function and identification of sensitive landuse types in Mangai City based on RWEQ model

Wen X, Zhen L (2020) Soil erosion control practices in the Chinese Loess Plateau: a systematic review. Environ Dev 34:100493. https://doi.org/10.1016/j.envdev.2019.100493

Williams JR (1990) The erosion-productivity impact calculator (EPIC) model: a case history. Philos Trans R Soc Lond B Biol Sci 329:421–428. https://doi.org/10.1098/rstb.1990.0184

Wischmeier WH, Smith DD (1965) Predicting rainfall-erosion losses from Cropland east of the Rocky Mountains

Wischmeier WH, Smith DD (1978) Predicting rainfall erosion losses: a guide to conservation planning. Department of Agriculture, Science and Education Administration

Woodruff NP, Siddoway FH (1965) A wind Erosion equation. Soil Sci Soc Am J 29:602. https://doi.org/10.2136/sssaj1965.03615995002900050035x

Wu G, Liu Y-F, Cui Z, Liu Y, Shi Z, Yin R, Kardol P (2020) Trade-off between vegetation type, soil erosion control and surface water in global semi-arid regions: a meta-analysis. J Appl Ecol 57:875–885. https://doi.org/10.1111/1365-2664.13597

Xia L, Bi R, Song X, Lv C (2021) Dynamic changes in soil erosion risk and its driving mechanism: a case study in the Loess Plateau of China. Eur J Soil Sci 72:1312–1331. https://doi.org/10.1111/ejss.13067

Xing L, Zhang F, Xing K, Li Y, Lu Q, Lu F (2021) Change of soil wind erosion and attribution in Bayannur, Inner Mongolia based on the revised wind Erosion equation. J Desert Res 41:111

Xu J, Xiao Y, Xie G, Wang Y, Jiang Y (2019) Computing payments for wind erosion prevention service incorporating ecosystem services flow and regional disparity in Yanchi County. Sci Total Environ 674:563–579. https://doi.org/10.1016/j.scitotenv.2019.03.361

Yang J, Huang X (2021) Earth Syst Sci Data 13:3907–3925. https://doi.org/10.5194/essd-13-3907-2021. The 30 m annual land cover dataset and its dynamics in China from 1990 to 2019

Yu M, Rui X, Xie W, Xu X, Wei W (2022) Research on Automatic Identification Method of terraces on the Loess Plateau Based on deep transfer learning. Remote Sens 14. https://doi.org/10.3390/rs14102446

Zhang WB, Fu JS (2003) Rainfall erosivity estimation under different rainfall amount. Resour Sci 25:35–41

Zhang G, Azorin-Molina C, Shi P, Lin D, Guijarro JA, Kong F, Chen D (2019) Impact of near-surface wind speed variability on wind erosion in the eastern agro-pastoral transitional zone of Northern China, 1982–2016. Agric Meteorol 271:102–115. https://doi.org/10.1016/j.agrformet.2019.02.039

Zhang X, She D, Huang X, Wang G (2020) Identifying the effects of land use changes and check dams on sediment yield in a watershed of the Loess Plateau, China. Authorea Prepr